A widespread family of ribosomal peptide metallophores involved in bacterial adaptation to copper stress

Laura Leprevost[#1], Sophie Jünger[#2], Guy Lippens[3], Céline Guillaume[2], Giuseppe Sicoli[4], Lydie Oliveira[5], Alex Rivera-Millot[1&], Gabriel Billon[4], Céline Henry[5], Rudy Antoine[*1], Svetlana Dubiley[*3], Séverine Zirah[*2], Yanyan Li[*2], Françoise Jacob-Dubuisson[*1]

[1] Univ. Lille, U1018-UMR9017-CIIL-Center for infection and Immunity of Lille, F-59000 Lille, FRANCE

[2] Unit Molecules of Communication and Adaptation of Microorganisms (MCAM), UMR 7245 CNRS, MNHN, 75005 Paris, FRANCE

[3] Toulouse Biotechnology Institute, CNRS/INRAE/INSA/UPS, 31077 Toulouse, FRANCE

[4] Univ. Lille, CNRS, UMR 8516 - LASIRE, Laboratoire de Spectroscopie pour les Interactions, la Réactivité et l'Environnement F-59000 Lille, FRANCE

[5] INRAE-AgroParisTech-Univ. Paris-Saclay, MICALIS, 78352 Jouy-en Josas, FRANCE

[#] contributed equally

[*] for correspondence: rudy.antoine@pasteur-lille.fr; svetlana.dubiley@gmail.com; severine.zirah@mnhn.fr; yanyanli@mnhn.fr; francoise.jacob@ibl.cnrs.fr

[&] current address: INRS-Centre Armand-Frappier Santé Biotechnologie, Bacterial Symbionts Evolution, Laval, Quebec H7V 1B7, Canada

Abstract

Ribosomally synthesized and post-translationally modified peptides (RiPPs) are a structurally diverse group of natural products that bacteria employ in their survival strategies. Herein, we characterized the mode of action, structure, and biosynthetic pathway of bufferins, products of mysterious 'gold-induced genes' (*gig)*-like operons. We show that bufferins form a new family of RiPPs ubiquitous in Eubacteria. Using *Caulobacter vibrioides* as a model organism, we elucidate the important role of bufferins in protecting bacteria from copper-induced stress. The cleavable N-terminal signal peptide guides bufferins export to the periplasm, where they efficiently sequester the copper ions. The metal-binding propensity of bufferins relies on the post-translational transformation of cysteine residues in the precursor peptide into 5-thioxazoles. This rare modification is installed by a multinuclear non-heme iron-dependent oxidative enzyme (MNIO, DUF692 family) in conjunction with its partner protein belonging to the DUF2063 family. Our study broadens the landscape of known peptide modifications installed by MNIO enzymes and unveils a widespread but overlooked bacterial copper defense strategy.

Synopsis: New copper-chelating natural peptide products with 5-thiooxazole modification installed by mutinuclear non-heme iron dependent oxidative enzyme, involved in bacterial adaptation to excess copper

51 ## Introduction

52 Several transition metals including copper are essential for living organisms [1, 2]. However, an
53 excess of copper is toxic to the cell notably due to the mismetallation of non-cognate proteins
54 that results in the inactivation of essential pathways [2-4]. Bacteria encounter copper in natural
55 habitats and within eukaryotic cells, which use it as a bactericidal agent [5, 6]. Therefore, they
56 have developed an arsenal of defense systems, including tight regulation of copper uptake,
57 various export systems, and sequestration/storage by copper-chelating molecules or proteins [7,
58 8]. For pathogens, these strategies are critical for host infection by enhancing their survival in
59 phagocytes, and hence they are linked to virulence [9].

60 Previous work on *Bordetella pertussis* has identified a four-gene operon controlled by the
61 master regulator of virulence, BvgAS [10]. This biosynthetic gene cluster (BGC) is similar to the
62 *gig* (gold-induced genes) operons of *Cupriavidus metallidurans* and *Legionella pneumophila*
63 and to a related operon of *Caulobacter vibrioides* [11-13] (Fig. 1A; Suppl. Fig. S1). The latter
64 operons are up-regulated upon exposure to transition metals, notably copper [11-14]. In particular,
65 the *C. vibrioides* operon is part of the few genes induced by copper in both swarmer and stalked
66 cells [14]. Although these data suggest a role for *gig*-like genes in copper stress response, the
67 nature and the function of produced molecules has remained a mystery. The *gig*-like operons
68 contain a gene encoding a DUF692 family protein, which was recently associated with the
69 biosynthesis of several ribosomally synthetized post-translationally modified peptides (RiPPs)
70 [15-21]. This suggests that the product of the *gig*-like operons could be also a post-translationally
71 modified peptide.

72 RiPPs are natural products with a tremendous variety of structures and biological activities
73 [22-24]. They are synthesized from a gene-encoded precursor peptide, generally composed of an
74 N-terminal leader sequence and a core sequence where post-translational modifications (PTMs)
75 occur. In many cases, a pathway-specific RiPP recognition element (RRE) domain interacts

with the leader sequence and mediates recruitment of the modification enzymes [25-27]. RRE domains are thus a hallmark feature of RiPP biosynthesis. The vast structural diversity of RiPPs is conferred by virtually unlimited possibilities of chemical transformations. An emerging family of PTM enzymes is the DUF692 family of multinuclear non-heme iron dependent oxidases (MNIOs) that catalyze various reactions in the biosynthesis of diverse RiPPs, mostly but not exclusively on Cys residues [15-21]. However, the full spectrum of reactions catalyzed by MNIOs remains far from being fully appreciated.

Here, using *C. vibrioides* as a model, we report the first functional and structural characterization of the molecules produced by *gig*-like operons. Our study unveiled that they represent a new family of RiPP metallophores, which contain a rare 5-thiooxazole modification of cysteine residues installed by MNIO enzymes. Based on our finding that the products of *gig*-like operons contribute to bacterial adaptation to toxic concentrations of copper by complexing with the excess metal, we named these RiPPs bufferins.

Results

Gig-like operons belong to putative RiPP BGCs. To gain insight into the gene function of *gig*-like operons, we performed an *in-silico* analysis on the CCNA_03363-03366 operon of *C. vibrioides*, hereafter named *buf1*. CCNA_03363 encodes a DUF2282-family protein (BufA1), whose members are 80-120 residues long and harbor four Cys residues (Cys^{I} to Cys^{IV}) and a predicted Sec-dependent signal peptide (Fig. 1A). We hypothesized that BufA1 is an unusually long precursor peptide whose translocation through the cytoplasmic membrane of the producing cell would rely on the ubiquitous Sec export pathway rather than on a specialized export pump encoded in its BGC as is often the case for other secreted RiPPs [28]. The AlphaFold2 model predicts that the BufA1 core peptide is likely to contain a 2-stranded β sheet and some α-helical structure (Suppl. Fig. S1). In the absence of PTMs, it would thus fold into a small protein, rather

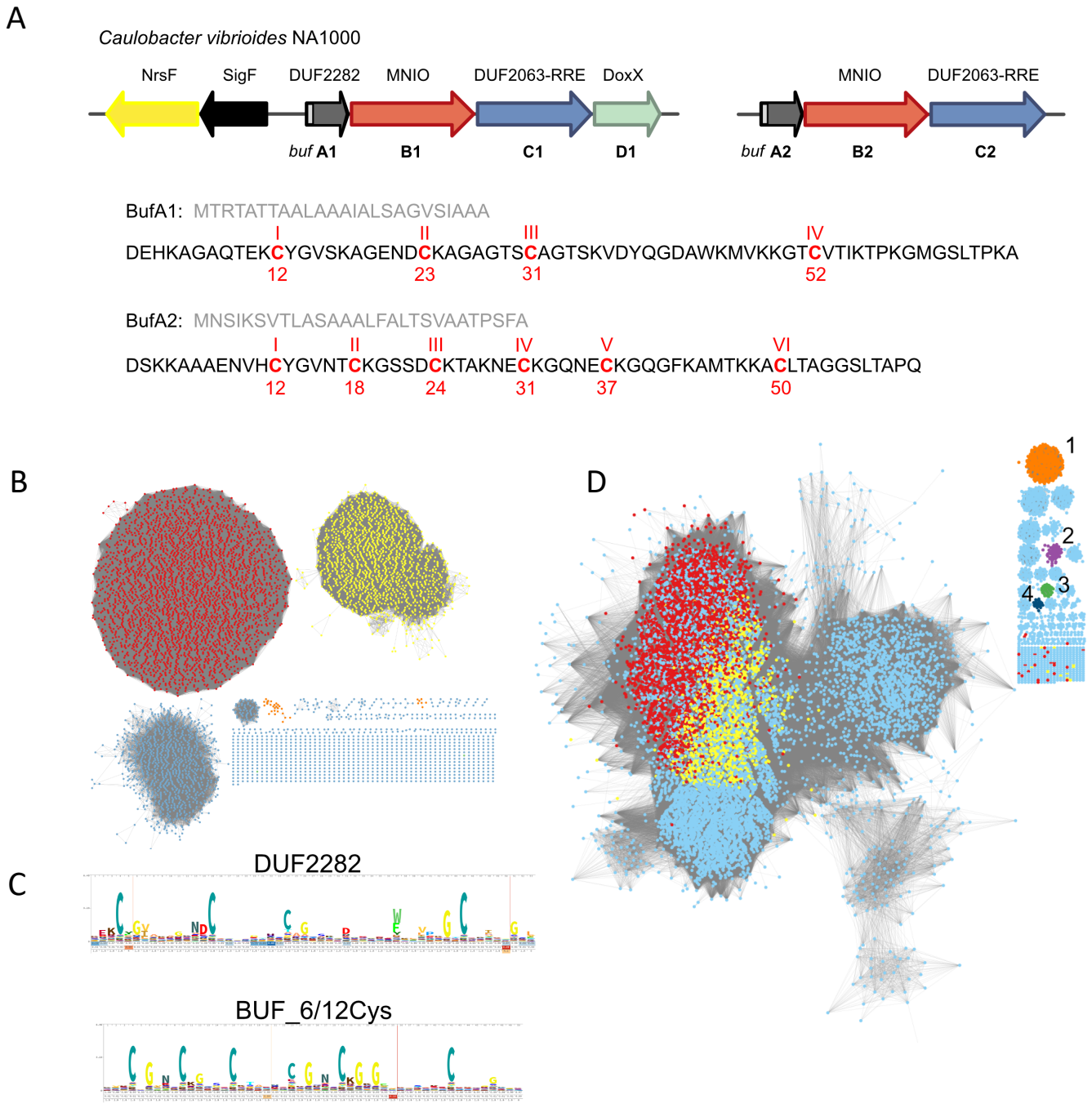

Figure 1. *In silico* analyses of the bufferin family. A. Gene composition of the *buf1* and *buf2* BGCs. The sequences of BufA1 and BufA2 are shown with the Cys residues labeled (numbering according to the core peptides). The signal peptide and core peptide sequences are in pale and dark grey, respectively. In anti-sense of *buf1ABCD* are genes coding for an extracellular-type sigma factor, SigF, and an anti-sigma factor, NrsF, that regulate *buf1* and *buf2* expression. **B**. SSN analyses of the putative signal peptide-containing bufferin-like precursors genetically associated with MNIOs. In the representative node network DUF2282 proteins, including BufA1 of *C. vibrioides*, belong to the largest cluster (red dots). The second largest cluster (yellow dots) represents BUF_6/12Cys proteins, which include BufA2 of *C. vibrioides*. The previously described MNIO-modified RiPPs of *Chryseobacterium* have predicted signal peptides and are found in two small clusters (in orange). **C**. Weblogos for the DUF2282 and BUF_6/12Cys bufferins. **D**. SSN analyses of MNIOs. In the representative node network (at 80% identity), MNIOs genetically associated with DUF2282 domain-containing proteins, including BufB1 of *C. vibrioides,* and with BUF_6/12Cys proteins, including BufB2 of *C. vibrioides*, are in red and yellow, respectively. MNIOs that modify other known RiPPs - methanobactins, *Chryseobacterium* RiPPs, TglA-type pearlins and aminopyruvatides - are found in small, distinct clusters numbered 1 to 4 and shown in purple, orange, green and dark blue dots, respectively.

101 than being a fully unstructured peptide. The product of CCNA_03364 (BufB1) is predicted to
102 belong to the MNIO family, whereas CCNA_03365 codes for a protein (BufC1) with an N-
103 terminal DUF2063 domain of unknown function. The structural model of BufC1 revealed that
104 its C-terminal domain is structurally related to RRE domains [25, 26, 27] (Suppl. Fig. S1). In light
105 of the recent discovery of MNIO enzymes involved in RiPP biosynthesis [15-21], we hypothesized
106 that BufB1 and BufC1 would install modifications on Cys residues of BufA1. Finally,
107 CCNA_03366 encodes a putative DoxX-type oxido-reductase (BufD1) [29, 30]. The other known
108 *gig*-like operons share the same gene organizations and predicted functions (Suppl. Fig. S1).

109 Inspection of the *C. vibrioides* genome identified a second operon, the *buf2* BGC
110 (CCNA_02999-03001) (Fig. 1A) which encodes homologs of BufB1 (CCNA_03000) and
111 BufC1 (CCNA_02999) but lacks a *doxX*-like gene. Its putative precursor peptide BufA2
112 (CCNA_03001) possesses a Sec-dependent signal peptide, like BufA1, but its core sequence
113 contains six rather than four Cys residues (Cys^{I} to Cys^{VI}) and is without family signature (Fig.
114 1A). The predicted 3D structure of the BufA2 core peptide adopts a very similar fold to that of
115 BufA1 (Suppl. Fig. S1).

116 To evaluate the prevalence of *gig*-like BGCs in prokaryotes, we collected >14,000 MNIO
117 protein sequences from the NCBI non-redundant database. The retrieved sequences were
118 widely distributed among Proteobacteria, Terrabacteria, Myxococcota,
119 Fibrobacteres/Chlorobi/Bacterioidetes, Planctomycetes/Verrucomicrobia/Chlamydia, and
120 Acidobacteriota groups (detailed *in silico* analyses will be published separately). We analyzed
121 their genomic contexts and collected associated genes coding for putative precursor peptides,
122 i.e., proteins smaller than 200 residues with Cys residues and a predicted N-terminal signal
123 peptide. In a sequence similarity network (SSN) constructed with those proteins, the largest
124 cluster corresponds to proteins with the DUF2282 signature, including *C. vibrioides* BufA1
125 (Fig. 1B). BufA2 of *C. vibrioides* belongs to the second largest cluster of proteins characterized

126 by six or twelve conserved Cys residues, which we named BUF_6/12Cys (Fig. 1B,C). Parallel
127 SSN analyses of the MNIO enzymes superfamily (Fig. 1D) showed that those associated with
128 DF2282 or BUF_6/12Cys bufferins belong to the most populated sequence cluster, distinct
129 from the smaller clusters of enzymes involved in the biosynthesis of methanobactins, RiPPs
130 from *Chryseobacterium*, TglA-type pearlins and amino-pyruvatides [15, 17-19, 21]. Together out
131 data indicate that bufferins currently form the largest group of RiPPs whose BGCs harbor
132 MNIO genes that are distinct from all previously described MNIO enzyme-modified RiPPs.
133
134 ***Bufferins are involved in adaptation to copper stress***. In *C. vibrioides*, *buf1* and *buf2* BGCs
135 belong to the SigF-controlled, core regulon of copper stress [12, 14, 31]. To test if they could be up-
136 regulated by other biologically relevant transition metals, we generated reporter fusions within
137 *bufA1* and *bufA2* and confirmed that both are induced by Cu^{2+} but not Fe^{2+}, Zn^{2+} or Mn^{2+} (Fig.
138 2A).
139 To determine if bufferins, the putative RiPP products of the *buf* BGCs, contribute to
140 adaptation to copper stress, we generated *C. vibrioides* deletion mutants that express a single
141 (Cv_{buf1} and Cv_{buf2}) or neither BGC (Cv_{DKO}). Cv_{DKO} grew more slowly than the parental Cv_{WT}
142 strain when $CuSO_4$ was added to the growth medium, unlike Cv_{buf1} or Cv_{buf2} (Fig. 2B). Thus,
143 bufferins enhance growth under copper stress and are functionally redundant. To confirm that
144 a single BGC is sufficient to protect bacteria from excess copper, we performed a gain-of-
145 function experiment in an *Escherichia coli* laboratory strain. For this, we expressed the
146 *buf1ABCD* operon under the control of a $P_{T5\text{-}lac}$ promoter upon IPTG induction. Expression of
147 *buf1ABCD* enhanced survival of *E. coli* exposed to a bactericidal concentration of $CuSO_4$ (Fig.
148 2C).
149 We then asked whether the protection from copper would confer an advantage on *C.*
150 *vibrioides* in biotic interactions. As amoeba notably use copper against their bacterial preys [5],

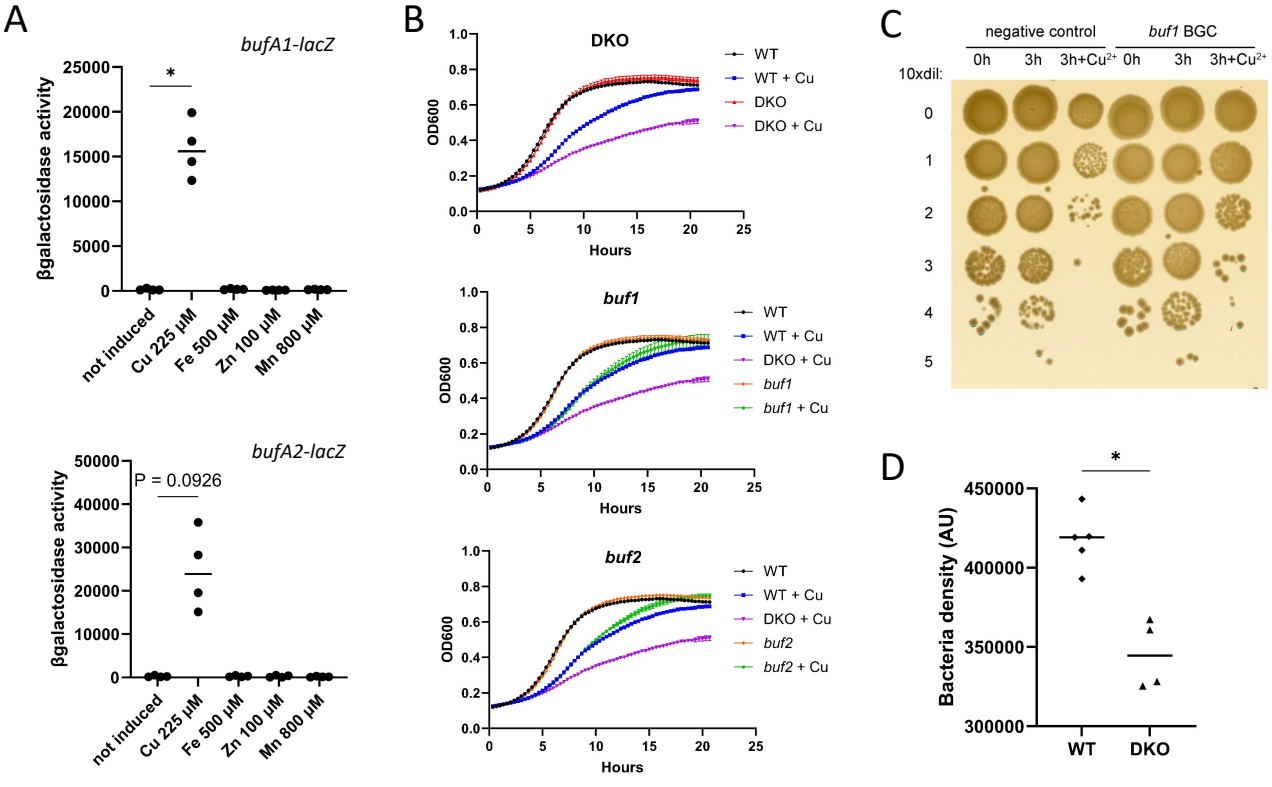

Figure 2. Regulation and function of the bufferins. **A**. Reporter assays with *bufA1-lacZ* and *bufA2- lacZ* transcriptional fusions. Bacteria were grown for 16 h with the indicated concentrations of $CuSO_4$, $FeSO_4$, $ZnSO_4$ or $MnCl_2$. All experiments were performed in biological quadruplicates, with three technical replicates. Non-parametric, one-way analysis of variance Kruskal-Wallis (two-sided) tests followed by a Dunn's multiple-comparison tests were used to analyze the differences between treatment with various compounds and the control (n=4; * in the upper left graph indicates p=0.047). **B**. Effect of copper on bacterial growth. The Cv_{DKO}, $Cv_{buf1ABCD}$ (*buf1)* and $Cv_{buf2ABC}$ (*buf2*) strains were grown without or with 225 µM $CuSO_4$, in biological quadruplicates. **C**. Gain-of-function assay. Expression of *buf1* in *E. coli* BL21(pCA24-buf1A^{str}BCD) was induced by IPTG, and the bacteria were challenged with 0.3 mM $CuSO_4$ for three hours before serial dilutions. BL21(pCA24-psmCA) expressing a non-relevant RiPP BGC was used as a control. **D**. Assay of bacterial lysis by *D. discoidum*. Bacterial densities of the lysis plaques were determined using ImageJ analyses. A non-parametric Mann-Whitney test (two-sided) was used to analyze the differences between the Cv_{WT} strain (n=5) and the Cv_{DKO} strain (n=4; * indicates p = 0.0159). The medians are shown (WT = 419,226 and DKO = 344,516) with a confidence interval of 96.83%. The ranks calculated were WT = 35 and DKO = 10.

151 a predation assay was performed. However, our attempts to measure survival of *C. vibrioides*
152 after ingestion by *Dictyostelium discoidum* were unsuccessful. Therefore, we tested if the
153 presence of the *buf* BGCs might slow down bacterial killing. We placed amoebal suspensions
154 onto bacterial lawns, and after incubation we determined bacterial densities in the contact zones
155 by densitometry scanning. Larger zones of complete bacterial clearance were observed for the
156 Cc_{DKO} than for the Cc_{WT} strain, consistent with a protective role of bufferins (Fig. 2D).
157
158 ***Characterization of PTMs of bufferins***. To identify the PTMs of bufferins, we engineered an
159 IPTG-inducible version of SigF to control expression of their BGCs in *C. vibrioides.* The
160 metabolic profiles of IPTG-treated Cv_{buf1}(pSigF) and Cv_{buf2}(pSigF) were analyzed by liquid
161 chromatography coupled to mass spectrometry (LC-MS) and compared to that of Cv_{DKO}(pSigF)
162 to reveal peptide species only present in the *buf*-expressing strains. In Cv_{buf1}(pSigF), a major
163 species exhibited a mass matching that of BufA1 with the Sec-dependent signal peptide cleaved
164 off and with a mass shift of -10 Da (Fig. 3A; Suppl. Fig. S2), suggesting that the core peptide
165 accumulates in the periplasm and contains post-translational modifications of one or more
166 residues. A second form with a mass shift of -12 Da was also detected, but not systematically,
167 and it disappeared upon freeze-thawing. The most stable product with a -10 Da mass shift is
168 considered the mature peptide product and named bufferin 1 (Buf1). Similarly, Cv_{buf2}(pSigF)
169 produced a major peptide product with a mass shift of -18 Da, called bufferin 2 (Buf2), and
170 another species with a -20 Da mass shift (Suppl. Figs. S2 and S3).
171 We speculated that mature bufferins contain modified Cys residues and disulfide (S-S)
172 bonds. To test this hypothesis, we performed reduction and alkylation treatment of the peptides.
173 This modification yielded species carrying three or four alkylated groups for Buf1 and four,
174 five or six alkylated groups for Buf2 (Suppl. Fig. S4), suggesting that the expected PTMs either
175 do not affect Cys residues or result in alkylation-sensitive groups. MS analyses of trypsin-

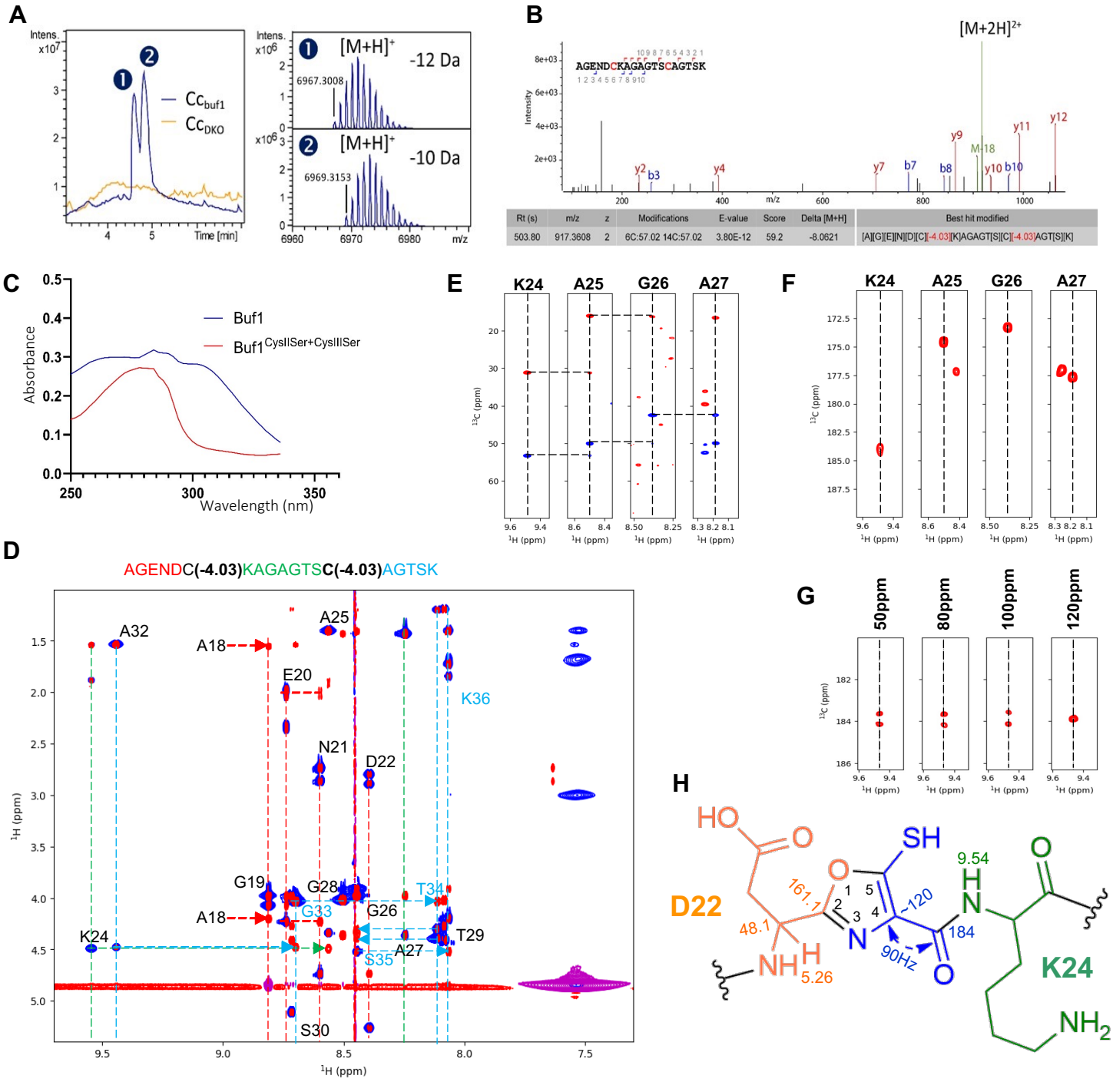

Figure 3. Post-translational modifications of bufferin 1. **A.** Top-down LC-MS analyses of cell extracts of Cv_{buf1}(pSigF) compared with Cv_{DKO}(pSigF). Left panel: total ion chromatograms, right panels: deconvoluted mass spectra of the two compounds detected only for Cv_{buf1}(pSigF). Their MW correspond to the core peptide (i.e. after removal of the signal peptide; calculated monoisotopic Mw=6978.35 Da), with mass shifts of -10 Da ($[M+H]^+$ at *m/z* 6969.32) and -12 Da ($[M+H]^+$ at *m/z* 6967.30). **B.** Bottom-up analysis of Buf1. MS/MS spectrum of the central tryptic peptide ($[M+2H]^{2+}$ at *m/z* 917.36). The two Cys residues carry carbamidomethyl groups resulting from alkylation with iodoacetamide (+ 57.02 Da), together with -4.03 Da mass shifts. **C.** UV/vis spectra of affinity-purified Buf1 and its Cys^{II}Ser+Cys^{III}Ser mutant version show an absorbance maximum at 305 nm for the first one only. **D.** NMR ROESY/TOCSY experiments to assign the resonances of the 19-mer peptide (Ala18-Lys36). **E**. HNCACB experiment on the uniformly ^{13}C, ^{15}N labeled 19-mer peptide: sequential walk for the sequence following Cys^{II} (Lys24-Ala27). For Lys24, we only identify its own Cα/Cβ carbons and no Cα/Cβ resonances of a preceding residue as is the case for the other residues. **F**. The HNCO planes at the ^{15}N frequency of the indicated residues show classical values around 175 ppm for all carbonyl resonances except for those residues downstream of a modified Cys, whose carbonyl carbons resonate at 184 ppm. **G**. HNCO planes through the resonance of Lys24 that immediately follows Cys23 (=Cys^{II}) while modifying the offset of the ^{13}C decoupling pulse during the C=O evolution period. Only when centered at 120 ppm, the 90-Hz carbon-carbon coupling is refocused. **H.** Measured NMR parameters and proposed structure for the bufferin 1 post-translational modifications (shown for Cys^{II}).

176 digested, alkylated bufferins revealed that in Buf1, Cys^{I} (Cys12) and Cys^{IV} (Cys52) (numbering
177 according to the core peptide, see Fig. 1) had mass increments corresponding to alkylation only,
178 indicative of unmodified residues (Suppl. Fig. S5). By contrast, in the central tryptic peptide
179 ^{18}AGENDCKAGAGTSCAGTSK^{36} containing Cys^{II} (Cys23) and Cys^{III} (Cys31), both Cys
180 residues carried mass increments corresponding to alkylation with additional -4.03 Da mass
181 shifts (Fig. 3B), as proposed by the untargeted PTM search solution SpecGlobX [32].

182 To confirm that Cys residues are required for the bufferin function, we constructed strains
183 with the four conserved Cys residues of Buf1 replaced with Ser, separately or in combinations.
184 In line with the proposed modifications of Cys^{II} or Cys^{III}, the substitution of any of the two with
185 Ser in Buf1 yielded peptides with mass shifts of -6 Da relative to the calculated mass of the
186 mutated peptide (Suppl. Fig. S6). We tested the ability of the mutated BufA1 to protect *C.*
187 *vibrioides* from excess copper. As expected, in the presence of $CuSO_4$ mutant strains grew more
188 slowly than the parental Cv_{buf1} (Suppl. Fig. S7), indicating the importance of both modified and
189 unmodified Cys residues for function. Altogether, the data are consistent with the presence of
190 an S-S bond between Cys^{I} and Cys^{IV} (resulting in -2 Da), and the central Cys^{II} and Cys^{III} being
191 targets of 4-electron oxidation reactions (-4 Da each) that generate alkylation-sensitive groups.
192 The minor Buf1 congener product with an overall mass shift of -12 Da would then correspond
193 to the formation of a labile S-S bond between the modified residues. Similarly, in Buf2, in
194 addition to the unmodified Cys^{I} (Cys24) and Cys^{VI} (Cys50) which might form an S-S bond
195 according to the AlphaFold2 model (Suppl. Fig. S1), the central Cys residues carry -4.03 Da
196 shifts (Suppl. Fig. S8).

197 To facilitate bufferin purification and further characterization of peptides, we added C-
198 terminal tags to BufA1. The affinity-purified tagged bufferin 1 was fully modified, displaying
199 -10 Da mass shifts relative to the calculated mass (Suppl. Fig. S9; Suppl. Table S1). To probe
200 if the modified Cys residues may be part of heterocycles as with other MNIO enzyme-catalyzed

201 PTMs [15, 18], we recorded UV-visible absorption spectra of purified Buf1 and the
202 Buf1$^{CysIISer+CysIIISer}$ variant. Indeed, consistent with the presence of aromatic heterocycles [33], the
203 spectrum of the former showed a broad absorbance peak extending to 310 nm, unlike that of
204 the latter (Fig. 3C). Similarly, the spectrum of recombinant Buf2 showed an absorbance
205 maximum at 305 nm (Suppl. Fig. S10).
206
207 ***Identification of the PTMs of bufferin 1 by NMR***. To increase the yield of bufferin for
208 structural elucidation by NMR, we co-expressed *bufA1* carrying an N-terminal His_6-SUMO-tag
209 with *bufB1* and *bufC1* in *E. coli*. Subsequent purification of modified BufA1 followed by
210 trypsin digestion and preparative HPLC allowed to obtain the central 19-mer peptide
211 encompassing Cys^{II} (Cys23) and Cys^{III} (Cys31) at a milligram scale (Suppl. Fig. S11). Its ^{1}H
212 spectrum indicated two groups of anomalous resonances (Suppl. Fig. S12). By combining
213 homonuclear ROESY and TOCSY experiments [34], they were assigned to the amide protons of
214 Lys24 and Ala32 that follow the modified Cys^{II} and Cys^{III} residues, respectively, and to the Hα
215 protons of Asp22 and Ser30 that precede them (Fig. 3D). Further analysis of the same spectra
216 showed the absence of both Hα and NH protons for the modified Cys residues. The absence of
217 the latter was verified on a natural abundance ^{1}H, ^{15}N HSQC spectrum (Suppl. Fig. S12). These
218 data suggest that their N and Cα atoms are part of heterocycles.
219 A ^{1}H, ^{13}C HSQC experiment showed correlations from the Asp22 and Ser30 Hα atoms to
220 their own Cα carbons at 48.1 and 52.4 ppm, respectively, which is 6 ppm higher than their
221 random coil values [35]. The ^{1}H, ^{13}C HMBC spectrum connected the same Hα protons to carbon
222 atoms at 161.1 ppm and 159.8 ppm, respectively (Suppl. Fig. S12). We produced a uniformly
223 ^{13}C,^{15}N-labeled modified BufA1 molecule in *E. coli* using the same expression system (Suppl.
224 Fig. S11), and we used its central tryptic peptide to obtain further carbon assignments on the
225 basis of triple-resonance NMR experiments [36, 37]. In the HNCACB experiment, we found no

226 resonances that could correspond to upstream neighbors for Lys24 or Ala32, confirming that
227 the Cα carbons of modified Cys^{II} and Cys^{III} do not resonate at the typical 50-ppm value
228 expected for Cys residues (Fig. 3E). In a HNCO experiment starting from the amide groups of
229 Lys24 or Ala32, we found values around 184 ppm for the C=O carbon atoms of both modified
230 Cys residues (Fig. 3F), far from 175-ppm and 200-ppm values expected for such atoms in
231 random-coil or thio-amide peptides, respectively [35, 38]. By increasing the resolution and varying
232 the offset of the decoupling pulse during the C=O evolution period, we determined a 90-Hz
233 coupling constant of both carbonyls with carbon atoms whose chemical shift is ~120 ppm,
234 consistent with their absence in the HNCACB experiment (Fig. 3G). Both parameters point to
235 the C=O carbon atoms of the modified Cys residues connected to carbon atoms in aromatic
236 rings [39].

237 When we compare the chemical shifts assigned on the modified BufA1 peptide with those
238 found for a 5-thiooxazole-containing natural product [33], we find the same 6-ppm upfield shift
239 of the Cα carbon of the preceding residue, the presence of similar carbon resonances at 120 and
240 160 ppm, and the 90-Hz coupling constant of the following carbonyl towards an aromatic ring
241 carbon. Together with the MS data and with the characteristic spectrophotometric absorbance
242 maximum at 305 nm [33], we conclude that the Buf1 modification implies cyclization of both its
243 central Cys residues to form thiooxazole groups (Fig. 3H).

244

245 ***Copper binding by bufferin 1.*** Given that heterocycles can be involved in copper binding [40],
246 we interrogated if bufferins can complex with copper, which could be the basis for their
247 protective effect. As our attempts to saturate bufferin 1 with copper *in vitro* proved to be
248 inefficient (Suppl. Fig. S13), we investigated complex formation *in vivo* by treating cultures of
249 *bufA1*-expressing *E. coli* with $CuSO_4$ for three hours prior to bufferin purification. Native MS
250 analysis showed that $Buf1^{str}$ thus produced was fully loaded with copper (Fig. 4A). Pulsed

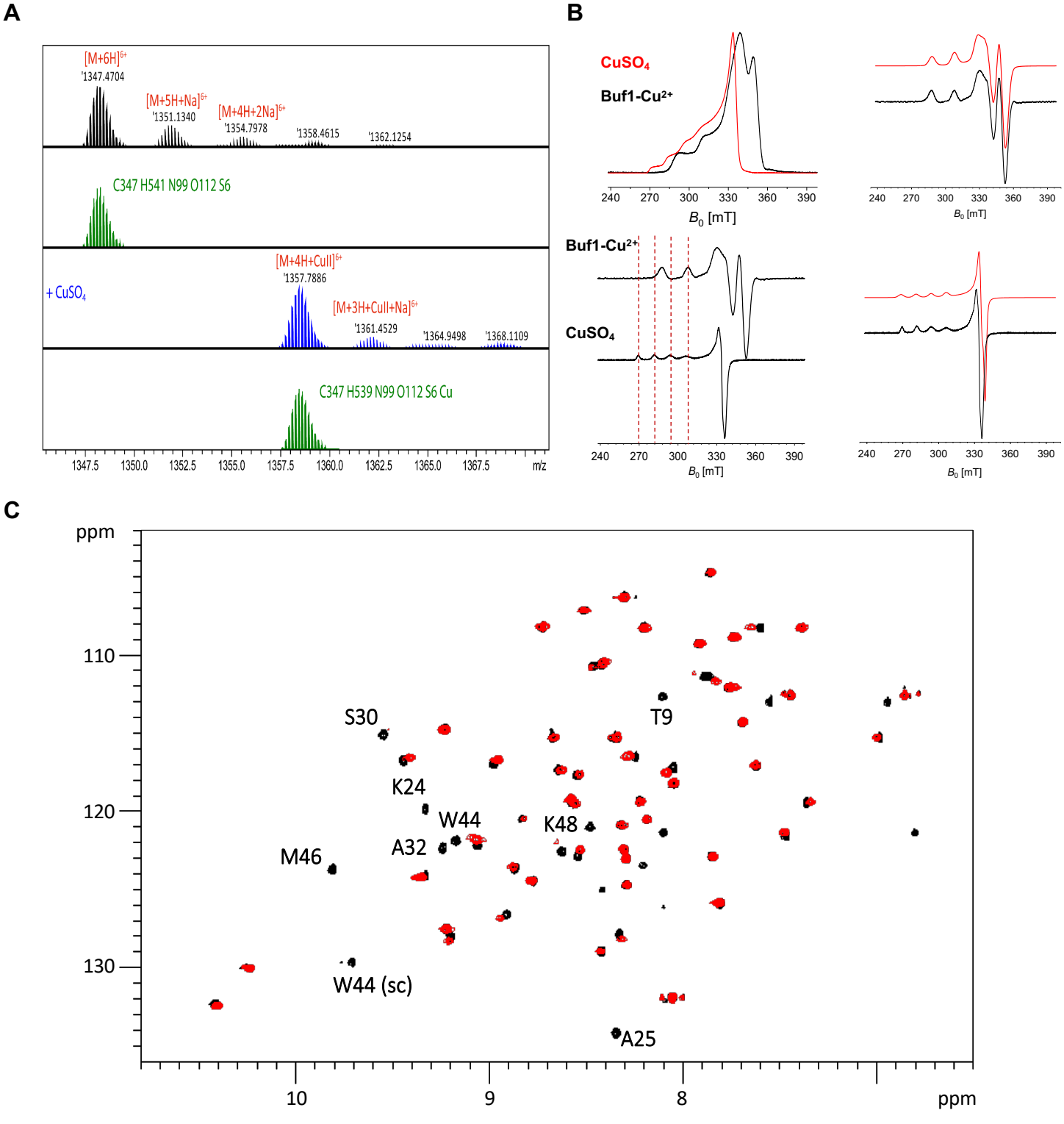

Figure 4. Analyses of the bufferin 1-copper complex formed *in vivo*. A. Native mass spectrometry analysis of purified Buf1^{str} loaded with Cu *in vivo*: isotopic patterns of the major charge state (6+). The upper two and lower two panels show Buf1^{str} from a non-supplemented culture and from cultures supplemented with $CuSO_4$, respectively. The calculated isotopic patterns for $[M+6H]^{6+}$ and $[M+4H+CuII]^{6+}$ species are shown in green. **B.** Evidence for Cu^{2+} binding to Buf1^{str} by EPR spectroscopy. Spectra of Echo-Detected Field-Swept (EDFS) of $CuSO_4$ (red line) and of the Buf1-Cu^{2+} complex (black line) are shown. Pseudo-modulation of the EDFS spectra is shown underneath. The panels at the right show the Easyspin fits (in red) and the experimental spectra (in black) for the Buf1-Cu^{2+} complex (top) and $CuSO_4$ (bottom). **C.** Superposition of the ^{1}H, ^{15}N HSQC spectra of apo bufferin (black peaks) and the *in-vivo* formed Buf1-Cu^{2+} complex (red peaks). sc= side chain.

251 electron paramagnetic resonance (EPR) spectra confirmed that Buf1 binds paramagnetic Cu^{2+},
252 and spectral simulations indicated coordinating N atoms [41] (Fig. 4B; Suppl. Tables S2 and S3).
253 To gain further insight into the copper binding site, we produced a ^{15}N,^{13}C-labeled Buf1
254 sample and recorded triple resonance spectra to assign its resonances. Simultaneously, we used
255 the ^{1}H, ^{15}N HSQC plane as a basis for HSQC-NOESY and TOCSY experiments to confirm the
256 assignments and gain some knowledge on structural aspects of the bufferin. The sequential
257 assignment was interrupted by the modified Cys residues, as expected. Interestingly, amide
258 resonances of the tryptic peptide and of the same segment in the full-length bufferin do not
259 correspond at all, suggesting that the full-length sequence imposes structural constraints on the
260 thiooxazole-containing loop. Part of these likely come from the β sheet spanning two short
261 strands in the structural model, Thr9-Tyr13 and Trp44-Lys48 (Suppl. Fig. S1), that we could
262 confirm experimentally through the strong Hα(i-1) – HN(i) NOE contacts between residues in
263 these segments and the cross-strand NOE contacts between the amide protons of Lys45 and
264 Cys12, and of Val47 and Glu10, respectively (Suppl. Fig. S14). PTMs of the Cys residues hence
265 do not interfere with the 3D structure predicted for the unmodified sequence.
266 A comparison of the spectra of the bufferin produced with or without copper showed that
267 whereas many peaks remained unchanged, some experienced a shift and some signal reduction,
268 and yet others disappeared altogether (Fig. 4C). The latter most probably concern residues close
269 to the paramagnetic Cu^{2+} ion. In particular, disappearance of the peaks corresponding to direct
270 neighbors of the thiooxazole heterocycles, such as Lys24, Ser30 and Ala32, confirms that the
271 heterocycles are involved in Cu^{2+} coordination. Interestingly, signals of Thr9, Trp44, Met46
272 and Lys48 predicted on the β-sheet face oriented towards the thiooxazole-containing loop also
273 disappeared in the spectrum of the Cu^{2+}-loaded Buf1. Whereas a full structural determination
274 of bufferin will require further experiments, our data support that the thiooxazole groups and
275 residues of the β sheet are involved in copper binding.

276

277 ***BufB1 and BufC1 are required for post-translational modification of bufferin.*** To dissect the
278 role of individual *buf* genes in the function of bufferins, we constructed Cv_{bufl} derivatives that
279 lack one or several genes and tested their growth phenotypes in the presence of $CuSO_4$. All
280 deletion strains except for that lacking *bufD1* displayed slow-growth phenotypes, showing that
281 BufA1, BufB1 and BufC1, but not BufD1, are required for function in these conditions (Fig.
282 5A).

283 To reveal the function of BufB1 in the bufferin maturation, we reconstituted the
284 modification reaction *in vitro* using the purified recombinant SUMO-BufA1, BufB1 and BufC1
285 proteins (Suppl. Fig. S15). Since MNIO enzymes require Fe^{II} and Fe^{III} ions for activity [17, 20],
286 BufB1 was analyzed by inductively coupled plasma - optical emission spectrometry, showing
287 the presence of two Fe ions. Structural alignments of a BufB1 model with the crystal structure
288 of MbnB of *Vibrio caribbeanicus*, an MNIO enzyme involved in methanobactin biosynthesis
289 [17] confirmed that the Fe-coordinating residues are conserved in BufB1. Next, BufA1 with the
290 SUMO-tag cleaved was incubated with BufB1 and/or BufC1. LC-MS analyses showed that
291 BufA1 was converted to a species with a -8 Da mass shift only when both BufB1 and BufC1
292 were present (Fig. 5B). Trypsin digestion of the *in vitro* modified BufA1 yielded the central 19-
293 residue fragment harboring the thiooxazole groups derived from Cys^{II} and Cys^{III} as confirmed
294 by MS/MS analyses (Fig. 5C). Together with the gene inactivation data, these experiments
295 established that BufB1 and BufC1 are required and sufficient to install the PTMs on BufA1.

296

297 ***The signal-peptide sequence is dispensable for heterocycle formation***. The particularity of
298 bufferin biosynthesis is that BufA precursors harbor a cleavable Sec-dependent export signal
299 peptide sequence at their N-terminus, which is an uncommon feature of bacterial RiPPs
300 precursors. We investigated if this sequence also acts as a leader peptide, required for Cys

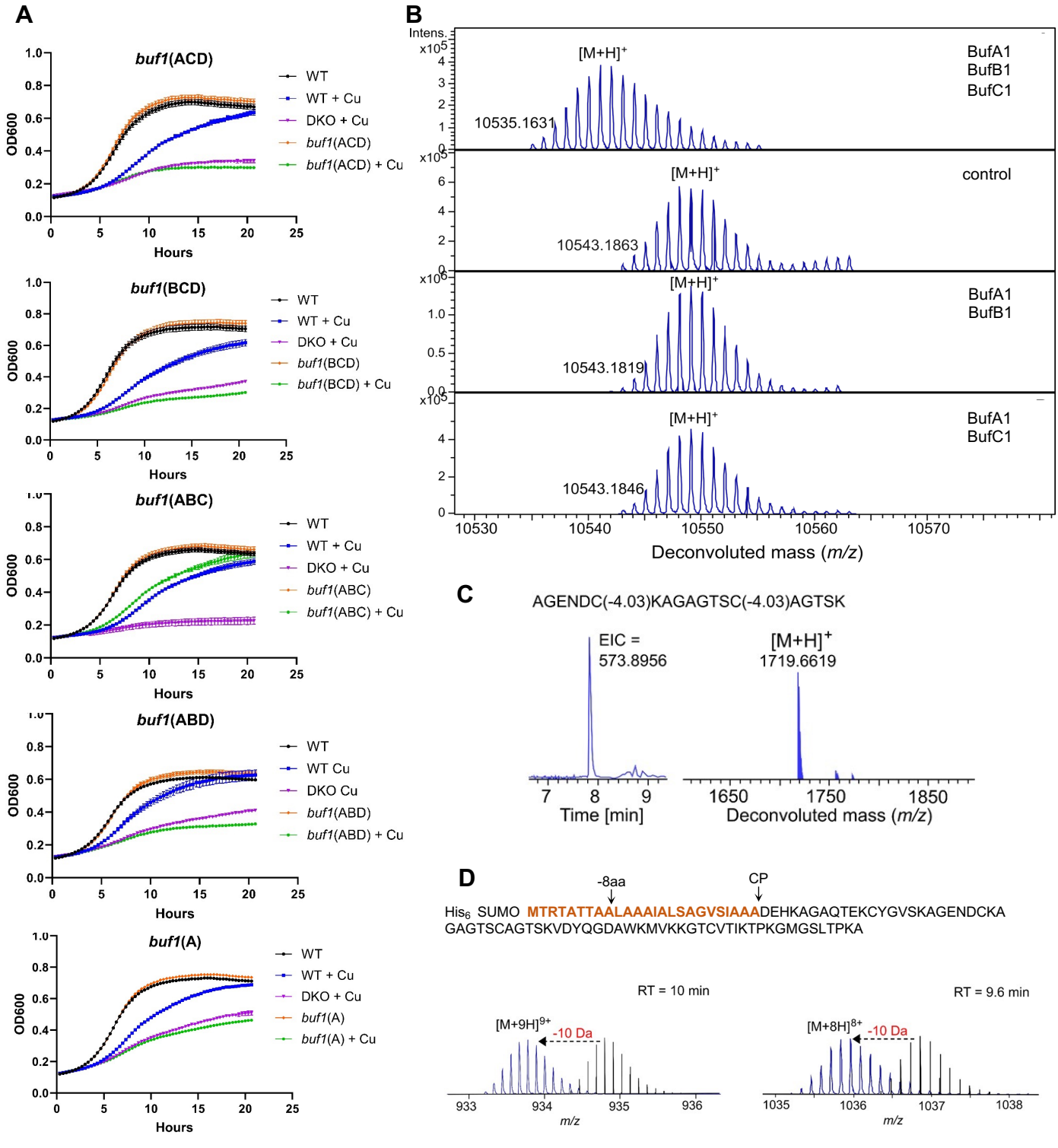

Figure 5. Biosynthesis of bufferin 1. A. Effect of Cu on the growth of *C. vibrioides* harboring various gene knock-outs in *buf1* BGC. All deletions were performed in Cv_{buf1}. Strains expressing the indicated genes were grown in PYE medium or in PYE medium containing 225 µM $CuSO_4$. **B.** *In vitro* reconstitution of the bufferin 1 biosynthesis. The deconvoluted mass spectra for the products of the *in vitro* reactions are shown, with the proteins added to the reactions indicated in the corresponding panels. The control reaction contained BufA1 and heat-denatured BufB1 and BufC1.
C. LC-MS analysis of the 19-residue tryptic fragment of the *in vitro* modified bufferin 1. The extracted ion chromatogram (EIC) of $[M+3H]^{3+}$ (at *m/z* 573.8945) and the deconvoluted mass are shown. **D**. Reconstitution of the system in heterologous host to address the role of the signal peptide for the PTMs. Schematic illustration of variant BufA1 with signal peptide truncations is shown on top. The signal peptide is in orange. *Left panel:* LC-MS analysis of modified BufA1(-8aa). MS spectrum of the most abundant charge state $[M+9H]^{9+}$, corresponding to a deconvoluted monoisotopic mass $[M+H]^{+}$ of 8391.1281 (blue) is compared to the theoretical spectrum of unmodified peptide (black). *Right panel*: LC-MS analysis of modified BufA1(CP). The MS spectrum of the most abundant charge state $[M+8H]^{8+}$, corresponding to a deconvoluted monoisotopic mass $[M+H]^{+}$ of 8277.9398 (blue) is compared to the theoretical spectrum of unmodified peptide (black).

301 transformation. Using the co-expression system of SUMO-*bufA1 with bufB1 and bufC1* in the
302 *E. coli* cytoplasm, the *bufA1* gene was mutated to generate variant precursors with the signal
303 peptide truncated eight residues from the N-terminus (BufA1(-8aa)) or completely removed
304 (BufA1(CP)). Subsequent LC-MS analysis of the purified BufA1 after SUMO cleavage
305 indicated that both truncated precursors were still modified with a 10 Da loss, consistent with
306 the presence of two thiooxazoles and one S-S bond (Fig. 5D). Thus, this data shows that the
307 signal peptide is dispensable for the installation of the PTMs.
308

309 **Discussion**

310 In this work, we solved a long-standing mystery by unveiling the chemical nature and function
311 of the products derived from heavy metal-induced *gig*-like operons found in various
312 environmental and pathogenic bacteria [11-13]. We showed that the products of *C. vibrioides gig*-
313 like operons are post-translationally modified peptides, bufferins, which protect bacteria from
314 copper stress by chelating excess metal. To the best of our knowledge, bufferins are the first
315 RiPPs directly purified from the producing organism that harbor 5-thiooxazole modifications.
316 The biosynthesis of bufferins involves several novel features. Firstly, bufferin precursor
317 peptides harbor Sec-dependent signal peptides instead of leader peptides at their N-terminus.
318 Although peptides with bulky modifications or macrocycles would most likely be poor
319 substrates for the Sec machinery due to the pore size of SecY [42], peptides with small
320 modifications could be exported this way if fused to a Sec-dependent signal peptide [43]. To our
321 knowledge, bufferins are the first RiPPs naturally exploiting Sec-dependent signals for efficient
322 translocation to the periplasm. The BufA1 signal peptide is dispensable for the heterocycles
323 installation in our heterologous system of expression, suggesting that determinants for the
324 specific recognition of the precursor peptide by the BufB1C1 modification machinery are
325 located within the core sequence. Secondly, transformation of Cys to 5-thiooxazole is catalyzed

326 by the MNIO enzyme BufB and its partner protein BufC, and not by a radical-SAM enzyme as
327 was recently reported [33]. Intense efforts have been made recently to explore the chemical space
328 of RiPPs involving MNIOs [15, 16, 19, 21, 44]. To date, members of this superfamily of enzymes are
329 known to catalyze remarkable oxidation reactions, including oxazolone coupled to thioamide
330 formation, excision of cysteine β-methylene, Cys-involved macrocyclization, and C-C and C-
331 N cleavages, as evidenced in the biosynthesis of methanobactins, TglA-type pearlins, RiPPs in
332 *Chryseobacterium*, aminopyruvatides, and methanobactin-like peptides in *Vibrio*, respectively
333 [15, 16, 19-21]. Our present study even further expands the reaction spectra of MNIO enzymes. In
334 line with previous work on Cys-modifying MNIO enzymes, BufB would similarly make use of
335 the mixed-valent iron center and proceed by an intermediate step of proton abstraction from the
336 Cβ of cysteine [17, 18, 20, 21] (Suppl. Fig. S16).

337 Using model bufferin systems, we demonstrated that the 5-thiooxazoles are key for the
338 copper-protecting function of bufferins. Noteworthy, formation of the bufferin-Cu^{2+} complex
339 was more efficient *in vivo* than *in vitro*. As expression of the bufferin BGC is triggered by the
340 presence of copper in the milieu, the bufferin is likely exposed to copper as soon as it emerges
341 in the periplasm. This can most likely not be faithfully reproduced *in vitro*.

342 Peptide natural products with other heterocycles are known to bind transition metals and
343 fulfil different functions [45-48]. Most prominently, the RiPP methanobactins scavenge copper
344 from the milieu to feed it to cuproenzymes, and some of them also protect bacteria from toxic
345 metals such as mercury [49]. The defensive role of bufferins is reminiscent of those of the non-
346 ribosomal peptides anthrochelin and yersiniabactin, which can passivate copper by chelation [50,
347 51]. The fate of copper ions bound by bufferins remains unknown. Periplasmic bufferins might
348 provide specific metallochaperones with copper for delivery to cuproproteins or alternatively
349 facilitate its export. Nevertheless, given the size and the diversity of the bufferin family, it is
350 tempting to speculate that some representatives could bind other transition metals.

351 Bufferins are part of complex and interwoven metal defense systems in bacteria and are
352 probably best seen as additional players that buttress active defense systems through copper
353 passivation under specific environmental conditions. Our data suggest that they are significant
354 contributors to the copper defense strategy of *C. vibrioides*. The presence of bufferin BGCs in
355 pathogenic bacteria indicates that they are likely also beneficial to the latter in host-pathogen
356 interactions, where they might help bacteria deal with copper encountered in phagosomal
357 compartments [5, 6, 52].

358 Our bioinformatic analyses indicated that bufferin precursors currently represent the largest
359 family of MNIO substrates, widespread in different bacterial phyla. The presence of signal
360 peptides in the precursors and the large sizes of their mature forms relative to most other RiPP
361 families confer them original properties. The diversity in length and sequence of the bufferin
362 cores provides bacteria with almost infinite possibilities to build natural peptide products
363 involved in adaptation to metal or other stresses.

364

365 **Supporting information**

366 This contains the complete Materials and Methods; diagrams for selected BGCs; Alphafold2
367 models; LC-MS and MS/MS spectra of BufA1, BufA2 and mutants; growth curves; 1D, HSQC,
368 HMBC, TOCSY-HSQC, ROESY-HSQC NMR spectra; protein gels; a mechanistic model;
369 Tables of sequences; EPR parameters; plasmids; strains; oligonucleotides and synthetic genes;
370 and references for this section.

371

372 **Acknowledgments.** We thank J.-M. Saliou for preliminary MS analyses and J.-Y. Matroule
373 and P. Cherry for providing *C. vibrioides* strains, plasmids and protocols. This project was
374 funded by the ANR grant CuRiPP (ANR-22-CE44-0001-02) to FJD. L. Leprevost and S. Jünger
375 were supported by PhD fellowships of Lille University and the French Ministry of Education

(ED 227 MNHN-SU), respectively. S. Dubiley was supported as a visiting scientist by a fellowship of the Collège de France. We thank the NMR facility of MetaToul (www.metatoul.fr). Metatoul is part of the French National Infrastructure for Metabolomics and Fluxomics MetaboHUB-AR-11-INBS-0010 (www.metabohub.fr), and is supported by the Région Midi-Pyrénées, the ERDF, the SICOVAL and the French Minister of Education & Research, who are all gratefully acknowledged. The LC-MS data were acquired at the MNHN bioorganic mass spectrometry platform and the PAPPSO platform (http://pappso.inra.fr/en). For the EPR experiments the financial support from the IR INFRANALYTICS FR2054 is acknowledged. ICP-OES measurements were performed by V. Alaimo on the Chevreul Institute Platform (U-Lille / CNRS). The Region Hauts de France and the French government are acknowledged for funding this apparatus.

References

1. Andrei, A.; Ozturk, Y.; Khalfaoui-Hassani, B.; Rauch, J.; Marckmann, D.; Trasnea, P. I.; Daldal, F.; Koch, H. G., Cu Homeostasis in Bacteria: The Ins and Outs. *Membranes (Basel)* **2020,** *10* (9).

2. Solioz, M., *Copper and Bacteria. Evolution, homeostasis and toxicity*. Springer Nature Switzerland AG: Cham, Switzerland, 2018.

3. Macomber, L.; Imlay, J. A., The iron-sulfur clusters of dehydratases are primary intracellular targets of copper toxicity. *Proc Natl Acad Sci U S A* **2009,** *106* (20), 8344-9.

4. Zuily, L.; Lahrach, N.; Fassler, R.; Genest, O.; Faller, P.; Seneque, O.; Denis, Y.; Castanie-Cornet, M. P.; Genevaux, P.; Jakob, U.; Reichmann, D.; Giudici-Orticoni, M. T.; Ilbert, M., Copper Induces Protein Aggregation, a Toxic Process Compensated by Molecular Chaperones. *mBio* **2022,** e0325121.

5. Hao, X.; Luthje, F.; Ronn, R.; German, N. A.; Li, X.; Huang, F.; Kisaka, J.; Huffman, D.; Alwathnani, H. A.; Zhu, Y. G.; Rensing, C., A role for copper in protozoan grazing - two billion years selecting for bacterial copper resistance. *Mol Microbiol* **2016,** *102* (4), 628-641.

6. Sheldon, J. R.; Skaar, E. P., Metals as phagocyte antimicrobial effectors. *Curr Opin Immunol* **2019,** *60*, 1-9.

7. Arguello, J. M.; Raimunda, D.; Padilla-Benavides, T., Mechanisms of copper homeostasis in bacteria. *Front Cell Infect Microbiol* **2013,** *3*, 73.

8. Chandrangsu, P.; Rensing, C.; Helmann, J. D., Metal homeostasis and resistance in bacteria. *Nat Rev Microbiol* **2017,** *15* (6), 338-350.

9. Hodgkinson, V.; Petris, M. J., Copper homeostasis at the host-pathogen interface. *J Biol Chem* **2012,** *287* (17), 13549-55.

410 10. Coutte, L.; Antoine, R.; Slupek, S.; Solans, L.; Derop, J.; Bonnefond, A.; Hot, D.; Locht, C.,
411 Combined RNAseq and ChIPseq Analyses of the BvgA Virulence Regulator of Bordetella pertussis.
412 *mSystems* **2020,** *5* (3).

413 11. Jwanoswki, K.; Wells, C.; Bruce, T.; Rutt, J.; Banks, T.; McNealy, T. L., The Legionella
414 pneumophila GIG operon responds to gold and copper in planktonic and biofilm cultures. *PLoS One* **2017,**
415 *12* (5), e0174245.

416 12. Kohler, C.; Lourenco, R. F.; Avelar, G. M.; Gomes, S. L., Extracytoplasmic function (ECF) sigma
417 factor sigmaF is involved in Caulobacter crescentus response to heavy metal stress. *BMC Microbiol* **2012,** *12*,
418 210.

419 13. Wiesemann, N.; Mohr, J.; Grosse, C.; Herzberg, M.; Hause, G.; Reith, F.; Nies, D. H., Influence
420 of copper resistance determinants on gold transformation by Cupriavidus metallidurans strain CH34. *J*
421 *Bacteriol* **2013,** *195* (10), 2298-308.

422 14. Maertens, L.; Cherry, P.; Tilquin, F.; Van Houdt, R.; Matroule, J. Y., Environmental Conditions
423 Modulate the Transcriptomic Response of Both Caulobacter crescentus Morphotypes to Cu Stress.
424 *Microorganisms* **2021,** *9* (6).

425 15. Ayikpoe, R. S.; Zhu, L.; Chen, J. Y.; Ting, C. P.; van der Donk, W. A., Macrocyclization and
426 Backbone Rearrangement During RiPP Biosynthesis by a SAM-Dependent Domain-of-Unknown-Function
427 692. *ACS Cent Sci* **2023,** *9* (5), 1008-1018.

428 16. Chioti, V. T.; Clark, K. A.; Ganley, J. G.; Han, E. J.; Seyedsayamdost, M. R., N-Calpha Bond
429 Cleavage Catalyzed by a Multinuclear Iron Oxygenase from a Divergent Methanobactin-like RiPP Gene
430 Cluster. *J Am Chem Soc* **2024**.

431 17. Dou, C.; Long, Z.; Li, S.; Zhou, D.; Jin, Y.; Zhang, L.; Zhang, X.; Zheng, Y.; Li, L.; Zhu, X.;
432 Liu, Z.; He, S.; Yan, W.; Yang, L.; Xiong, J.; Fu, X.; Qi, S.; Ren, H.; Chen, S.; Dai, L.; Wang, B.;
433 Cheng, W., Crystal structure and catalytic mechanism of the MbnBC holoenzyme required for
434 methanobactin biosynthesis. *Cell Res* **2022,** *32* (3), 302-314.

435 18. Kenney, G. E.; Dassama, L. M. K.; Pandelia, M. E.; Gizzi, A. S.; Martinie, R. J.; Gao, P.; DeHart,
436 C. J.; Schachner, L. F.; Skinner, O. S.; Ro, S. Y.; Zhu, X.; Sadek, M.; Thomas, P. M.; Almo, S. C.;
437 Bollinger, J. M., Jr.; Krebs, C.; Kelleher, N. L.; Rosenzweig, A. C., The biosynthesis of methanobactin.
438 *Science* **2018,** *359* (6382), 1411-1416.

439 19. Nguyen, D. T.; Zhu, L.; Gray, D. L.; Woods, T. J.; Padhi, C.; Flatt, K. M.; MItchell, D. A.; van
440 der Donk, W. A., Biosynthesis of macrocyclic peptides with C-terminal beta-amino-alpha-keto acid groups
441 by three different metalloenzymes. *BioRxiv* **2024**.

442 20. Park, Y. J.; Jodts, R. J.; Slater, J. W.; Reyes, R. M.; Winton, V. J.; Montaser, R. A.; Thomas, P.
443 M.; Dowdle, W. B.; Ruiz, A.; Kelleher, N. L.; Bollinger, J. M., Jr.; Krebs, C.; Hoffman, B. M.; Rosenzweig,
444 A. C., A mixed-valent Fe(II)Fe(III) species converts cysteine to an oxazolone/thioamide pair in
445 methanobactin biosynthesis. *Proc Natl Acad Sci U S A* **2022,** *119* (13), e2123566119.

446 21. Ting, C. P.; Funk, M. A.; Halaby, S. L.; Zhang, Z.; Gonen, T.; van der Donk, W. A., Use of a
447 scaffold peptide in the biosynthesis of amino acid-derived natural products. *Science* **2019,** *365* (6450), 280-
448 284.

449 22. Arnison, P. G.; Bibb, M. J.; Bierbaum, G.; Bowers, A. A.; Bugni, T. S.; Bulaj, G.; Camarero, J.
450 A.; Campopiano, D. J.; Challis, G. L.; Clardy, J.; Cotter, P. D.; Craik, D. J.; Dawson, M.; Dittmann, E.;
451 Donadio, S.; Dorrestein, P. C.; Entian, K. D.; Fischbach, M. A.; Garavelli, J. S.; Goransson, U.; Gruber,
452 C. W.; Haft, D. H.; Hemscheidt, T. K.; Hertweck, C.; Hill, C.; Horswill, A. R.; Jaspars, M.; Kelly, W. L.;
453 Klinman, J. P.; Kuipers, O. P.; Link, A. J.; Liu, W.; Marahiel, M. A.; Mitchell, D. A.; Moll, G. N.; Moore,
454 B. S.; Muller, R.; Nair, S. K.; Nes, I. F.; Norris, G. E.; Olivera, B. M.; Onaka, H.; Patchett, M. L.; Piel,
455 J.; Reaney, M. J.; Rebuffat, S.; Ross, R. P.; Sahl, H. G.; Schmidt, E. W.; Selsted, M. E.; Severinov, K.;
456 Shen, B.; Sivonen, K.; Smith, L.; Stein, T.; Sussmuth, R. D.; Tagg, J. R.; Tang, G. L.; Truman, A. W.;
457 Vederas, J. C.; Walsh, C. T.; Walton, J. D.; Wenzel, S. C.; Willey, J. M.; van der Donk, W. A., Ribosomally
458 synthesized and post-translationally modified peptide natural products: overview and recommendations for
459 a universal nomenclature. *Nat Prod Rep* **2013,** *30* (1), 108-60.

460 23. Li, Y.; Rebuffat, S., The manifold roles of microbial ribosomal peptide-based natural products in
461 physiology and ecology. *J Biol Chem* **2020,** *295* (1), 34-54.

462 24. Montalban-Lopez, M.; Scott, T. A.; Ramesh, S.; Rahman, I. R.; van Heel, A. J.; Viel, J. H.;
463 Bandarian, V.; Dittmann, E.; Genilloud, O.; Goto, Y.; Grande Burgos, M. J.; Hill, C.; Kim, S.; Koehnke,
464 J.; Latham, J. A.; Link, A. J.; Martinez, B.; Nair, S. K.; Nicolet, Y.; Rebuffat, S.; Sahl, H. G.; Sareen, D.;
465 Schmidt, E. W.; Schmitt, L.; Severinov, K.; Sussmuth, R. D.; Truman, A. W.; Wang, H.; Weng, J. K.;
466 van Wezel, G. P.; Zhang, Q.; Zhong, J.; Piel, J.; Mitchell, D. A.; Kuipers, O. P.; van der Donk, W. A.,
467 New developments in RiPP discovery, enzymology and engineering. *Nat Prod Rep* **2021,** *38* (1), 130-239.

468 25. Burkhart, B. J.; Hudson, G. A.; Dunbar, K. L.; Mitchell, D. A., A prevalent peptide-binding domain
469 guides ribosomal natural product biosynthesis. *Nat Chem Biol* **2015,** *11* (8), 564-70.

470 26. Chekan, J. R.; Ongpipattanakul, C.; Nair, S. K., Steric complementarity directs sequence
471 promiscuous leader binding in RiPP biosynthesis. *Proc Natl Acad Sci U S A* **2019,** *116* (48), 24049-24055.

472 27. Kloosterman, A. M.; Shelton, K. E.; van Wezel, G. P.; Medema, M. H.; Mitchell, D. A., RRE-
473 Finder: a Genome-Mining Tool for Class-Independent RiPP Discovery. *mSystems* **2020,** *5* (5).

474 28. Severi, E.; Thomas, G. H., Antibiotic export: transporters involved in the final step of natural
475 product production. *Microbiology (Reading)* **2019,** *165* (8), 805-818.

476 29. Müller, F. H.; Bandeiras, T. M.; Urich, T.; Teixeira, M.; Gomes, C. M.; Kletzin, A., Coupling of
477 the pathway of sulphur oxidation to dioxygen reduction: characterization of a novel membrane-bound
478 thiosulphate:quinone oxidoreductase. *Mol Microbiol* **2004,** *53* (4), 1147-60.

479 30. Nambi, S.; Long, J. E.; Mishra, B. B.; Baker, R.; Murphy, K. C.; Olive, A. J.; Nguyen, H. P.;
480 Shaffer, S. A.; Sassetti, C. M., The Oxidative Stress Network of Mycobacterium tuberculosis Reveals
481 Coordination between Radical Detoxification Systems. *Cell Host Microbe* **2015,** *17* (6), 829-37.

482 31. Alvarez-Martinez, C. E.; Baldini, R. L.; Gomes, S. L., A caulobacter crescentus extracytoplasmic
483 function sigma factor mediating the response to oxidative stress in stationary phase. *J Bacteriol* **2006,** *188* (5),
484 1835-46.

485 32. Prunier, G.; Cherkaoui, M.; Lysiak, A.; Langella, O.; Blein-Nicolas, M.; Lollier, V.; Benoist, E.;
486 Jean, G.; Fertin, G.; Rogniaux, H.; Tessier, D., Fast alignment of mass spectra in large proteomics datasets,
487 capturing dissimilarities arising from multiple complex modifications of peptides. *BMC Bioinformatics* **2023,**
488 *24* (1), 421.

489 33. Lewis, J. K.; Jochimsen, A. S.; Lefave, S. J.; Young, A. P.; Kincannon, W. M.; Roberts, A. G.;
490 Kieber-Emmons, M. T.; Bandarian, V., New Role for Radical SAM Enzymes in the Biosynthesis of
491 Thio(seleno)oxazole RiPP Natural Products. *Biochemistry* **2021,** *60* (45), 3347-3361.

492 34. Wüthrich, K., *NMR of proteins and nucleic acids.* Wiley: New York, 1986.

493 35. Wishart, D. S.; Bigam, C. G.; Holm, A.; Hodges, R. S.; Sykes, B. D., 1H, 13C and 15N random
494 coil NMR chemical shifts of the common amino acids. I. Investigations of nearest-neighbor effects. *J Biomol*
495 *NMR* **1995,** *5* (1), 67-81.

496 36. Sattler, M., Heteronuclear multidimensional NMR experiments for the structure determination of
497 proteins in solution employing pulsed field gradients. *Progr. Nucl. Magn. Reson. Spectr.* **1999,** *34*, 93-158.

498 37. Yamazaki, T.; Lee, W.; Arrowsmith, C. H.; Muhandiram, D. R.; Kay, L. E., A Suite of Triple
499 Resonance NMR Experiments for the Backbone Assignment of 15N, 13C, 2H Labeled Proteins with High
500 Sensitivity. *J. Am. Chem. Soc.* **1994,** *116*, 11655-11666.

501 38. Fiore, K. E.; Patist, M. J.; Giannakoulias, S.; Huang, C. H.; Verma, H.; Khatri, B.; Cheng, R. P.;
502 Chatterjee, J.; Petersson, E. J., Structural impact of thioamide incorporation into a beta-hairpin. *RSC Chem*
503 *Biol* **2022,** *3* (5), 582-591.

504 39. Wray, V., Progress in NMR Spectroscopy. 1979; Vol. 13, pp 177-256.

505 40. Kenney, G. E.; Rosenzweig, A. C., Chalkophores. *Annu Rev Biochem* **2018,** *87*, 645-676.

506 41. Bennett, B.; Kowalski, J. M., EPR Methods for Biological Cu(II): L-Band CW and NARS. *Methods*
507 *Enzymol* **2015,** *563*, 341-61.

508 42. Bonardi, F.; Halza, E.; Walko, M.; Du Plessis, F.; Nouwen, N.; Feringa, B. L.; Driessen, A. J.,
509 Probing the SecYEG translocation pore size with preproteins conjugated with sizable rigid spherical
510 molecules. *Proc Natl Acad Sci U S A* **2011,** *108* (19), 7775-80.

511 43. Kuipers, A.; Wierenga, J.; Rink, R.; Kluskens, L. D.; Driessen, A. J.; Kuipers, O. P.; Moll, G. N.,
512 Sec-mediated transport of posttranslationally dehydrated peptides in Lactococcus lactis. *Appl Environ*
513 *Microbiol* **2006,** *72* (12), 7626-33.

514 44. Clark, K. A.; Seyedsayamdost, M. R., Bioinformatic Atlas of Radical SAM Enzyme-Modified RiPP
515 Natural Products Reveals an Isoleucine-Tryptophan Crosslink. *J Am Chem Soc* **2022,** *144* (39), 17876-17888.

516 45. DiSpirito, A. A.; Semrau, J. D.; Murrell, J. C.; Gallagher, W. H.; Dennison, C.; Vuilleumier, S.,
517 Methanobactin and the Link between Copper and Bacterial Methane Oxidation. *Microbiol Mol Biol Rev* **2016,**
518 *80* (2), 387-409.

519 46. Kenney, G. E.; Rosenzweig, A. C., Methanobactins: Maintaining copper homeostasis in
520 methanotrophs and beyond. *J Biol Chem* **2018,** *293* (13), 4606-4615.

521 47. Li, Y.; Ma, Y.; Xia, Y.; Zhang, T.; Sun, S.; Gao, J.; Yao, H.; Wang, H., Discovery and biosynthesis
522 of tricyclic copper-binding ribosomal peptides containing histidine-to-butyrine crosslinks. *Nat Commun*
523 **2023,** *14* (1), 2944.

524 48. Semrau, J. D.; DiSpirito, A. A.; Obulisamy, P. K.; Kang-Yun, C. S., Methanobactin from
525 methanotrophs: genetics, structure, function and potential applications. *FEMS Microbiol Lett* **2020,** *367* (5),
526 fnaa045.

527 49. Baral, B. S.; Bandow, N. L.; Vorobev, A.; Freemeier, B. C.; Bergman, B. H.; Herdendorf, T. J.;
528 Fuentes, N.; Ellias, L.; Turpin, E.; Semrau, J. D.; DiSpirito, A. A., Mercury binding by methanobactin
529 from Methylocystis strain SB2. *J Inorg Biochem* **2014,** *141*, 161-169.

530 50. Büttner, H.; Hörl, J.; Krabbe, J.; Hertweck, C., Discovery and biosynthesis of anthrochelin, a
531 growth-promoting metallophore of the human pathogen *Luteibacter anthropi*. *ChemBioChem* **2023,** *24*,
532 e202300322.

533 51. Koh, E. I.; Robinson, A. E.; Bandara, N.; Rogers, B. E.; Henderson, J. P., Copper import in
534 Escherichia coli by the yersiniabactin metallophore system. *Nat Chem Biol* **2017,** *13* (9), 1016-1021.

535 52. Chaturvedi, K. S.; Henderson, J. P., Pathogenic adaptations to host-derived antibacterial copper.
536 *Front Cell Infect Microbiol* **2014,** *4*, 3.

537